Eur. Phys. J. B **6**, 355–362 (1998)

THE EUROPEAN PHYSICAL JOURNAL B

Induced ferrielectricity in antiferroelectric liquid crystals

A.A. Boulbitch[1] and P. Tolédano[2]

[1] Technical University of Munich, Laboratory of Biophysics E22, James-Franck Street 85747 Garching, Germany
[2] Département de Physique, Université d'Amiens, 80000 Amiens, France

Received: 23 October 1997 / Revised: 8 April 1998 / Accepted: 14 July 1998

Abstract. The behaviour of the antiferroelectric SmC_A liquid crystal phase under applied electric field is discussed theoretically. The phase diagram involving the SmA, SmC_A and SmC_A^* phases is worked out and shown to exhibit a Lifshitz critical point. The deformation of the bilayer structures induced by the field transforms the SmC_A phases into a ferrielectric phase whose specific configuration is described.

PACS. 64.70.Md Transitions in liquid crystals – 61.30.Cz Theory and models of liquid crystal structure

1 Introduction

A number of experimental studies have recently clarified some of the questions which have been raised by the discovery of antiferroelectric and ferrielectric phases in liquid crystals [1–6]. On the one hand, quasielastic light scattering [7], and X-ray experiments [8] have established the bilayer structure of the antiferroelectric SmC_A^* phase in MHPOBC {4-(1-methylheptyloxycarbonyl)-phenyl-4'-octyloxybiphenyl-4-carboxylate}. On the other hand, the relaxational behaviour of the SmC_A^* and SmC_γ^* phases was carefully investigated [9–13] revealing complex absorption processes corresponding to three normal and phason modes, attributed to the antiferroelectric ordering, to azimuthal fluctuations of the molecules and to the slow rotation of the double twisted helicoidal modulation wave of the antiferroelectric structure, restoring the translational symmetry lost at the SmA–SmC_A^* transition.

One of the important aspects, which has been only partly elucidated by the experimental investigations [14–19], is the behaviour of the antiferroelectric structure under application of an electric field. Here, one can expect a competition between two phenomena: the unwinding of the antiferroelectric helices, resulting in a commensurate lock-in SmC_A phase, or the onset of a field induced SmC^* phase. Besides, as the SmC_A–SmC^* transition is found in non-racemic mixtures, *i.e.* with unequal numbers N_L and N_R of left and right handed molecules, the relative composition $x = (N_L - N_R)/2(N_L + N_R)$ influences differently the order of stabilization of the structures. For example, in TFMHPOBC{4-(1,1,1-trifluoromethyl-heptiloxycarbonyl)phenyl-4'-octyl-oxybiphenyl-4-carboxylate) [16]} the SmA–SmC_A^* transition occurs in the nearly optically pure substance, whereas for inhomogeneous compositions the sequence SmA–SmC^*–SmC_A^* is realized.

The present work aims to analyze, in the framework of a Landau-type model, the behaviour of an antiferroelectric SmC_A phase under applied electric field E for non-racemic compositions. At first the effect of E on the SmA–SmC_A transition in examined (Sect. 2). The phase diagram involving SmA, SmC_A and SmC_A^* phases is worked out (Sect. 3). The deformation of the local structure of the SmC_A phase under the effect of E is then shown to correspond to a ferrielectric structure whose molecular organization is described (Sect. 4).

2 Phenomenological theory of the SmA–SmC_A^* phase transition under applied electric field

2.1 Basic ingredients of the model

One can describe phenomenologically a bilayer stacking of dipolar molecules by using the formalism introduced in references [20,21], which makes use of two axial vectors $\boldsymbol{\eta}_1$ and $\boldsymbol{\eta}_2$ defined as follows:

$$\boldsymbol{\eta}_1 = (-n_{1y}n_{1z}, n_{1x}n_{1z}), \boldsymbol{\eta}_2 = (-n_{2y}n_{2z}, n_{2x}n_{2z})$$

where the $n_{iu}(i = 1, 2; u = x, y, z)$ are the components of the director in the ith layer, and the space variables x, y and z, indicate, respectively, the in-plane coordinates and the direction perpendicular to the layers. The four components of $\boldsymbol{\eta}_1$ and $\boldsymbol{\eta}_2$ span a four-dimensional reducible representation of the parent chiral SmA space-group: $G_0 = D_\infty \otimes T_z$. This representation decomposes in two irreducible representations of G_0 which are, respectively, spanned by the planar vectors: $\boldsymbol{\eta}_p = \boldsymbol{\eta}_1 + \boldsymbol{\eta}_2$, and $\boldsymbol{\eta}_A = \boldsymbol{\eta}_1 - \boldsymbol{\eta}_2$ transforming as the in-layer polarization: $\mathbf{p} = \mathbf{p}_1 + \mathbf{p}_2$ and antipolarization $\mathbf{a} = \mathbf{p}_1 - \mathbf{p}_2$ where $\mathbf{p}_1$ and $\mathbf{p}_2$ are the polarizations of two adjacent smectic layers. Using the symmetry properties of $\mathbf{p}$ and $\mathbf{a}$ one can

therefore construct the free-energy expansion:

$$\Phi = \int [\tilde{\Phi}_H(\mathbf{p},\mathbf{a}) + \tilde{\Phi}_{grad}(\mathbf{p},\mathbf{a})] S dz \tag{1}$$

where S is the area of the layer surfaces. $\tilde{\Phi}_H$ and $\tilde{\Phi}_{grad}$ are the homogeneous and, gradient parts of the expansion density, defined as [20,21]:

$$\tilde{\Phi}_H = \frac{\alpha_1}{2}p^2 + \frac{\alpha_2}{2}a^2 + \frac{\beta_1}{2}p^4 + \frac{\beta_2}{2}a^4 + \frac{\gamma_1}{2}p^2a^2 + \frac{\gamma_2}{2}(\mathbf{p}\cdot\mathbf{a})^2 - (\mathbf{p}\cdot\mathbf{E}) \tag{2}$$

and:

$$\tilde{\Phi}_{grad} = \frac{g_1}{2}\Big[(\frac{\partial p_x}{\partial z})^2 + (\frac{\partial p_y}{\partial z})^2\Big] + \frac{g_2}{2}\Big[(\frac{\partial a_x}{\partial z})^2 + (\frac{\partial a_y}{\partial z})^2\Big] + \frac{\lambda_1}{2}(p_x\frac{\partial p_y}{\partial z} - p_y\frac{\partial p_x}{\partial z}) + \frac{\lambda_2}{2}(a_x\frac{\partial a_y}{\partial z} - a_y\frac{\partial a_x}{\partial z}) \tag{3}$$

where $\alpha_1,\ \alpha_2,\ \beta_1,\ \beta_2,\ \gamma_1,\ \gamma_2,\ g_1,\ g_2,\ \lambda_1,\ \lambda_2$ are phenomenological coefficients, with $(\beta_1,\ \beta_2,\ g_1,\ g_2) > 0$. $\mathbf{E}$ is an applied electric field.

In reference [21], the tilt angle of the molecules was assumed to remain constant across the antiferro, ferro and ferrielectric phases, as the regions of stability of these phases were taken far from the region of stability of the SmA phase, and only the azimuthal angle of the molecules, with respect to the normal to the layers, was considered. As we aim here to describe the SmA–SmC$^*_A$ transition, the tilt-angle of the molecules is the primary order-parameter. As a consequence, the minimization of Φ requires to work out the more general solutions of the corresponding Euler-Lagrange equations, which have been discussed previously by Zeks *et al.* [22]. Note that higher-order couplings of the form $(\mathbf{p}\cdot\mathbf{E})^2$ or $(\mathbf{a}\cdot\mathbf{E})^2$ are not taken into account into equation (2) since they do not modify in a qualitative way the results obtained from our model. Note also that the Lifshitz invariants in equation (3), which express the helicity of the structures, cannot be neglected as in reference [20], since the helicity is high for SmA* phases observed in optically pure substances.

2.2 Behaviour of the basic structures for a chiral compound

Let us consider a system undergoing a direct SmA–SmC$^*_A$ transition, assuming that it occurs far from the region of stability of the SmC* phase. Hence one can neglect the quartic p-term in equation (2) and the square gradient p-term in equation (3), since these terms express small perturbations in the considered region. Consequently no stable ferroelectric or ferrielectric phase will be stabilized. One can introduce the auxiliary variables:

$$\mathbf{A} = (\beta_2 g_2)^{1/2}\lambda_2^{-1}\cdot\mathbf{a} \quad \text{and} \quad \mathbf{P} = g_2\lambda_2^{-2}(\beta_2\alpha_1)^{1/2}\cdot\mathbf{p}. \tag{4}$$

The order parameter expansion defined by equation (1) becomes: $\Phi = \lambda_2^3\beta_2^{-1}g_2^{-1}SF$ with:

$$F = \int \Big[\frac{\alpha}{2}(A_x^2 + A_y^2) + \frac{1}{4}(A_x^2 + A_y^2) + \frac{1}{2}(P_x^2 + P_y^2) + \frac{1}{2}G_1(P_x^2 + P_y^2)(A_x^2 + A_y^2) + \frac{1}{2}G_2(A_xP_x + A_yP_y)^2 + \frac{1}{2}(\dot{A}_x^2 + \dot{A}_y^2) + \frac{1}{2}(A_x\dot{A}_y - A_y\dot{A}_x) - hP_x\Big]du \tag{5}$$

$\alpha = \alpha_2 g_2 \lambda_2^{-2}$ and $G_{1,2} = \lambda_2^2\gamma_{1,2}(\beta_2 g_2\alpha_1)^{-1}$ are renormalized constants, $u = \lambda_2 g_2^{-1} z$ is the renormalized coordinate and $\mathbf{h} = g_2\lambda_2^{-2}(\beta_2\alpha_1^{-1})^{1/2}$. $\mathbf{E}$ the renormalized field, which is assumed to be applied along the Ox axis. $\dot{A}_u = \partial A/\partial u$. The functional F depends only on the three independent phenomenological coefficients α, G_1 and G_2 and on the field $\mathbf{h}$.

A first step in finding the form of F is to consider only the homogeneous terms in equation (5). The equations of state of the system correspond in this case to the minimization of the polynomial F with respect to A_x, A_y, P_x and P_y. Three phases are found to be possibly stable:

1) A SmA phase with an induced polarization $P_x = h$, and $P_y = A_x = A_y = 0$. Note that this phase actually correspond to a field-induced SmC* phase whose tilt angle and polarization go to zero at the limit $h = 0$. In this article we will nevertheless denominate this phase SmA.

2) Two distinct homogeneous (commensurate) antiferroelectric phases denoted SmC$_{A_1}$ and SmC$_{A_2}$. The equations of state for the SmC$_{A_1}$ phase are:

$$P_x + G_1P_xA_y^2 = h, \ \text{ and } \ \alpha A_y + A_y^3 + G_1P_x^2A_y = 0 \tag{6}$$

which yield: $P_x \neq 0,\ A_y \neq 0,\ P_y = A_x = 0$. The equations of state for the SmC$_{A_2}$ phase are:

$$P_x + (G_1 + G_2)P_xA_x^2 = h, \quad \text{and} \quad \alpha A_x + A_x^3 + (G_1 + G_2)P_x^2A_x = 0 \tag{7}$$

which give: $P_x \neq 0, A_x \neq 0, P_y = A_y = 0$.

The stability conditions for the three preceding phases are:

$$\alpha + (G_1 + G_2)h^2 \geq 0, \quad \text{and} \quad \alpha + G_1h^2 \geq 0 \tag{8}$$

which show that for $G_2 < 0$, the SmC$_{A_2}$ phase is stabilized below the SmA phase, whereas for $G_2 > 0$ it is the SmC$_{A_1}$ phase which appears first. Thus, for a given sign of G_2 only one of the two antiferroelectric structures will take place below the SmA phase. As the phase diagram possesses analogous features for $G_2 < 0$ or $G_2 > 0$, we will consider only this latter case, namely the SmA–SmC$_{A_1}$ phase transition. Using equation (6) one can then write the corresponding stability condition under the reduced form:

$$\alpha + G_1P_{x1}^2 + 3A_{y1}^2 \geq 0 \tag{9}$$

where P_{x1} and A_{y1} are the equilibrium values of P_x and A_x in the SmC$_{A_1}$ phase. At a second-order phase transition

between the SmA and SmC_{A_1} phases, one has $A_{y1} = 0$ and $P_{x1} = h$. Accordingly, the equation of this second-order transition line in the $\alpha - h$ plane is:

$$\alpha + G_1 h^2 = 0. \tag{10}$$

In the vicinity of the preceding line one can expand $P_{x1} = h(1 + G_1 A_y^2)^{-1}$ in series of A_{y1}:

$$P_{x1} \simeq h(1 - G_1 A_{y1}^2 + G_1^2 A_{y1}^4 - G_1^3 A_{y1}^6 + \cdots). \tag{11}$$

Substituting (11) into (5), one gets the following form for F:

$$F = \frac{1}{2}(\alpha + G_1 h^2) A_{y1}^2 + \frac{1}{4}(1 - 2G_1^2 h^2) A_{y1}^4 + \frac{1}{2} G_1^3 h^2 A_{y1}^6 - \frac{1}{2} h^2. \tag{12}$$

For small values of h the SmA–SmC_{A_1} transition is second order, while for $h \geq h_{tcp}$ the transition becomes first-order. The coordinates of the tricritical point are:

$$h_{tcp} = \frac{1}{G_1 \sqrt{2}}, \quad \text{and} \quad \alpha_{tcp} = -\frac{1}{2G_1}\cdot \tag{13}$$

For $h < h_{tcp}$ one can omit the sixth degree term in (12) and obtain the explicit form for A_{y1} and for the equilibrium value of F:

$$A_{y1} \simeq \left[(\alpha + G_1 h^2)/(2G_1^2 h^2 - 1)\right]^{1/2}, \quad \text{and}$$
$$F_{eq} \simeq (\alpha + G_1 h^2)^2/4(2G_1^2 h^2 - 1) - \frac{1}{2} h^2. \tag{14}$$

Writing $\alpha_2 = a_2^0(T - T_{c2})$ and assuming α_1 constant, one can express, using (4), the equations of the transition lines and critical point in the $T - \mathbf{E}$ phase-diagram, which is shown in Figure 1a. Figure 1b represents the field dependence of the antiferroelectric component A_{y1} given by equation (14). We will now use the preceding results as a basis for investigating the more complex behaviour of the helicoidal antiferroelectric structure with an external electric field.

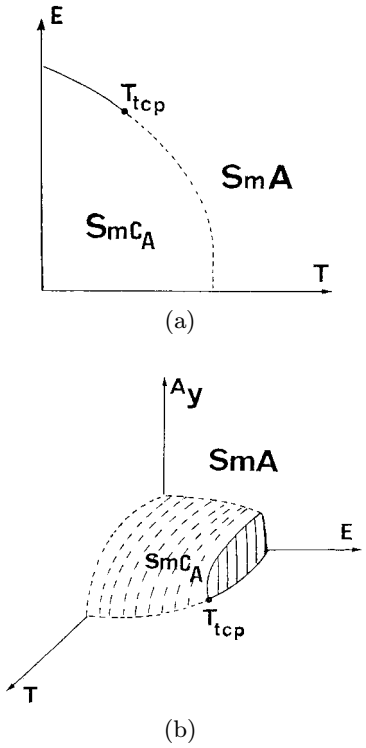

Fig. 1. (a) Temperature-electric field phase diagram of a system containing a basic unwound antiferroelectric structure, from equation (10). (b) Dependence on field and temperature of the antiferroelectric component A_{y1} from equation (14). Dashed and solid lines are, respectively, second and first-order transition lines.

2.3 Helicoidal antiferroelectric structures

For non-racemic mixtures, the gradient invariants in (5) must be taken into account for the minimization of the functional F as inhomogeneous (incommensurate) states can be stabilized. The influence of the gradient terms on the stability of the homogeneous SmA and SmC_{A_1} phases is found by considering the bifurcations induced in the system of Euler-Lagrange equations, which minimize F. The more general solutions of these equations can be written [24], as periodic perturbations of the form:

$$P_x = P_{x_1} + \hat{p}_1 \cos(qu + \omega), \quad P_y = \hat{p}_2 \sin(qu + \omega),$$
$$A_x = \hat{a}_1 \cos(qu), \quad A_y = A_{y_1} + \hat{a}_2 \sin(qu) \tag{15}$$

where $\hat{p}_1, \hat{p}_2, \hat{a}_1$ and $\hat{a}_2$ are the (small) amplitudes describing the overcritical behaviour of the order-parameters $\mathbf{P}$ and $\mathbf{A}$ below the bifurcation. ω is a phase factor and q is the wave-vector of the perturbations. Substituting (15) into F one gets, after integration of the sum (5) over a period $2\pi/q$:

$$\begin{aligned} F_1 = {} & 2\pi\Big[\frac{\alpha}{2} A_{y_1}^2 + \frac{1}{4} A_{y_1}^4 + \frac{1}{2} P_{x_1}^2 + \frac{1}{2} G_1 P_{x_1}^2 A_{y_1}^2 - P_{x_1} h\Big] \\ & + \frac{\pi}{2}\Big[\hat{a}_1^2 |\alpha + q^2 + A_{y_1}^2 + (G_1 + G_2) P_{x_1}^2| + \hat{a}_2^2 |\alpha \\ & + q^2 + 3A_{y_1}^2 + G_1 P_{x_1}^2| + 2q\hat{a}_1\hat{a}_2 + \hat{p}_1^2 + \hat{p}_2^2 + \frac{1}{4}\hat{a}_1^2\hat{a}_2^2\Big] \\ & + \frac{3}{8}(\hat{a}_1^4 + \hat{a}_2^4) + |G_1 \hat{p}_1^2 + (G_1 + G_2)\hat{p}_2^2| A_{y_1}^2 \\ & + 2A_{y_1} P_{x_1} \sin\theta (G_2 \hat{a}_1 \hat{p}_2 - 2G_1 \hat{a}_2 \hat{p}_1) \\ & + \frac{1}{4}(G_1 + G_2)(2 + \cos 2\theta)(\hat{p}_1^2 \hat{a}_1^2 + \hat{p}_2^2 \hat{a}_2^2) \\ & + \frac{1}{2} G_2 \hat{a}_1 \hat{a}_2 \hat{p}_1 \hat{p}_2 \cos 2\theta + \frac{1}{4} G_1 (2 - \cos 2\theta)(\hat{p}_1^2 \hat{a}_2^2 + \hat{p}_2^2 \hat{a}_1^2). \end{aligned} \tag{16}$$

F_1 is the Landau expansion which describes the phase transitions from the homogeneous SmA phase to the inhomogeneous or homogeneous antiferroelectric phases. The stable states are obtained by a minimization of F_1 with respect to $A_{y1}, P_{x1}, \hat{p}_1, \hat{p}_2, \hat{a}_1, \hat{a}_2$ an ω. The loss of stability of the homogeneous phase figuring in the phase diagram, with respect to the inhomogeneous phase, is expressed by

the condition:

$$D(A_{y1}, P_{x1}, q, \omega) = 0 \tag{17}$$

where D represents the determinant of the matrix of the second derivatives of F_1 with respect to the perturbative variables $\hat{p}_1, \hat{p}_2, \hat{a}_1, \hat{a}_2$. The explicit form of equation (17) can be written:

$$q^4 + d_2 q^2 + d_0 = 0 \tag{18}$$

with

$$d_2 = 2\alpha + 4A_{y1}^2 + (2G_1 + G_2)P_{x1}^2 - \Big\{4G_1^2(1 + G_1 A_{y1}^2)^{-1} + G_2^2\Big[1 + (G_1 + G_2)A_{y1}^2\Big]^{-1}\Big\}A_{y1}^2 P_{x1}^2 - 1 \tag{19}$$

and:

$$d_0 = \left[\alpha + A_{y1}^2 + (G_1 + G_2)P_{x1}^2 - \frac{G_2^2 A_{y1}^2 P_{x1}^2 \sin^2\omega}{1 + (G_1 + G_2)A_{y1}^2}\right] \times \left[\alpha + 3A_{y1}^2 + G_1 P_{x1}^2 - \frac{4G_1^2 A_{y1}^2 P_{x1}^2 \sin^2\omega}{1 + G_1 A_{y1}^2}\right]. \tag{20}$$

A loss of stability of a homogeneous phase will occur for the wave-vector q_c, which determines the absolute minimum of D with respect to q and ω. Minimization of D with respect to q yields:

$$4d_0 = d_2^2 \tag{21}$$

which constitutes the equation of the limit of stability line for the homogeneous phases. The critical wave-vector on this line is:

$$q_c = \Big(-\frac{1}{2}d_2\Big)^{1/2} \tag{22}$$

which shows that $d_2 < 0$. When $d_2 = 0$ on the limit of stability line $q_c = 0$. In other words, *one has a crossover from a transition to a inhomogeneous phase to a transition to a homogeneous phase.* The double condition:

$$d_2 = q_c = 0 \tag{23}$$

corresponds to the coordinates of a Lifshitz point [25] in the $T-\mathbf{E}$ phase diagram. Minimization of D with respect to ω gives:

$$\frac{\partial D}{\partial(\sin^2\theta)}\sin 2\omega = 0$$

and

$$\frac{\partial^2 D}{\partial(\sin^2\theta)^2}\sin^2 2\omega + 2\frac{\partial D}{\partial\theta}\cos 2\omega > 0. \tag{24}$$

It is easy to show that conditions (24) coincide with a minimum of D for

$$\cos\omega = 0 \tag{25}$$

whereas $\sin\omega = 0$ is associated with a maximum of D. Introducing (22, 25) in (15) provides *the equilibrium values of the order-parameter components in the inhomogeneous phases*, close to the limit of stability of the homogeneous phase.

Starting from the SmA phase, for which $P_{x1} = h$, and $A_{y1} = 0$, the equation of the limit of stability line is:

$$\alpha_0(h) = \frac{1}{4}(G_2^2 h^4) - \frac{1}{2}(2G_1 + G_2)h^2 + \frac{1}{4}\cdot \tag{26}$$

For $\alpha < \alpha_0(h)$ an helicoïdal $\mathrm{SmC}^*_{A_1}$ phase takes place. The wave-vector associated with the pitch of the helix is:

$$q_c = \frac{1}{2}(1 - G_2^2 h^4)^{1/2}. \tag{27}$$

with increasing field h, q_c decreases and vanishes at the Lifshitz point of coordinates:

$$\alpha_L = -G_1/G_2, \quad h_L = G_2^{-1/2}. \tag{28}$$

At this point the $\mathrm{SmC}^*_{A_1}$ phase transforms into the SmC_{A_1} phase, the two preceding phases merging with the SmA phase at the Lifshitz point. These results are valid for $d_2 < 0$, namely for $-h_L < h < h_L$. The perturbative approach expressed in equation (15) holds only for small values of the amplitudes $\hat{p}_1, \hat{p}_2, \hat{a}_1, \hat{a}_2$, so one can assume that the Lifshitz point takes place at lower fields than the tricritical point on the SmA–SmC_{A_1} transition line. This condition corresponds to the inequality: $G_2 < 2G_1^2$. Accordingly, the limit of stability line (26) coincides with a second-order transition line between the SmA and $\mathrm{SmC}^*_{A_1}$ phases.

Similar considerations apply to the loss of stability of the SmC_{A_1} phase with respect to the $\mathrm{SmC}^*_{A_1}$ phase. However, due to the absence of group-subgroup relationship between these phases the SmC_{A_1}–$\mathrm{SmC}^*_{A_1}$ transition is first-order. Furthermore equation (22), which represents a limit of stability line for the SmC_{A_1} phase, cannot be simplified, as P_{x1} and A_{y1} have non-zero values in the SmC_{A_1} phase. Nevertheless, one can approximate equation (22) in two extreme regions of the phase diagram: *close to* the Lifshitz point at which end simultaneously the SmC_{A_1}–$\mathrm{SmC}^*_{A_1}$ transition line and the limit of stability line (21), and *far from* the Lifshitz point, where only the two, SmC_{A_1} and $\mathrm{SmC}^*_{A_1}$, phases are found. The two situations will be discussed separately.

3 Temperature-electric field phase diagram

Let us consider the $\mathrm{SmC}^*_{A_1}$ phase in the vicinity of the SmA–$\mathrm{SmC}^*_{A_1}$ transition, namely for $\alpha \lesssim \alpha_0(h)$. As in equation (16) the coefficient of $\hat{p}_1^2$ and $\hat{p}_2^2$ are all positive, below the transition one has $\hat{p}_1 = \hat{p}_2 = 0$. The structure of the SmC^*_A phase will thus be exclusively determined by the non-zero perturbative order-parameter amplitudes $\hat{a}_1$ and $\hat{a}_2$. Following the approach proposed by Michelson and Cabib [26], one can diagonalize the quadratic remaining terms in F_1, using the transformation:

$$\begin{aligned}\nu &= \hat{a}_1 - (G_2 h^2 - \Delta)(2q)^{-1}\hat{a}_2,\\ \mu &= \hat{a}_1 - (G_2 h^2 + \Delta)(2q)^{-1}\hat{a}_2\end{aligned} \tag{29}$$

with $\Delta = (G_2^2 h^4 + 4q^2)^{1/2}$. The matrix of the quadratic form of the harmonic part of F_1 possesses two eigenvalue,

and the SmA–SmC$^*_{A_1}$ transition occurs when the smallest of these eigenvalues goes to zero. The parameter μ corresponds to this critical eigenvalues, and one has in the vicinity of the transition $\mu \gg \nu$, so it is possible to assume that $\nu \simeq 0$. Introducing the *critical order-parameter*:

$$\xi = \mu(\Delta - G_2 h^2/\Delta)^{1/2}. \tag{30}$$

one gets the effective Landau expansion associated with the SmA($\xi = 0$)–SmC$^*_{A_1}$($\xi \neq 0$) transition:

$$F_1(\xi, h) = \frac{\pi}{2}(\frac{1}{2}\lambda\xi^2 + \epsilon\xi^4) - \pi h^2 \tag{31}$$

with: $\lambda = \frac{1}{2}\left[2\alpha + 2q^2 + (2G_1 + G_2)h^2 - (G_2^2 h^4 + 4q^2)^{1/2}\right]$ and $\epsilon = (\Delta - G_2 h^2)^2(2\Delta^2 + G_2^2 h^2)\left[32\Delta^2(\Delta^2 - G_2 h^2)^2\right]^{-1}$. The equation of the SmA–SmC$^*_{A_1}$ transition line, and the corresponding critical wave-vector q_c are, respectively, given by $\lambda = 0$ and by $\partial\lambda/\partial q = 0$, which yield again the expressions (26, 27). In the vicinity of the Lifshitz point, as q is small, one can use for λ and ϵ the following approximations:

$$\lambda(h, q) \simeq \alpha + G_1 h^2 + q^2(1 - h_L^2/h^2) + q^4 h_L^6/h^6 \tag{32}$$

and $\epsilon \simeq 3/32$. Replacing q by its critical value (27). F_1 becomes:

$$F_1(\xi, h) = \frac{\pi}{2}\left[\frac{1}{2}(\alpha - \alpha_0(h))\xi^2 + \frac{3}{32}\xi^4\right] - \pi h^2. \tag{33}$$

The minimization of F_1 with respect to ξ, gives $\xi = 0$ for $\alpha > \alpha_0$ (the SmA phase), and:

$$\xi_A = \pm\left[-\frac{8}{3}(\alpha - \alpha_0(h)\right]^{1/2} \tag{34}$$

for $\alpha < \alpha_0(h)$ (the SmC$^*_{A_1}$ phase). The equilibrium values of $\hat{a}_1$ and $\hat{a}_2$ are:

$$\hat{a}_1 = \pm\left[\frac{2}{3}(1 - G_2 h^2)|\alpha - \alpha_0(h)|\right]^{1/2},$$
$$\hat{a}_2 = \mp\left[\frac{2}{3}(1 + G_2 h^2)|\alpha - \alpha_0(h)|\right]^{1/2}. \tag{35}$$

They give in turn the equilibrium value of F_1 in the SmC$^*_{A_1}$ phase:

$$F_1^{eq} = -\frac{\pi}{3}\left[\alpha - \alpha_0(h)\right]^2 - \pi h^2. \tag{36}$$

The equation of the first-order SmC$_A$–SmC$^*_{A_1}$ transition line, close to the Lifshitz point, is obtained from the condition $F_1^{eq} = F_{eq}$, where F_{eq} is given by equation (14). It yields the equation:

$$\alpha(h) = \alpha_L - 2G_1 h_L(h - h_L) - (h - h_L^2)/(K - 1) \tag{37}$$

where $K = (2/3)(1 - 2G_1^2/G_2)^{1/2} > 1$. Equation (37) is valid only in the vicinity of the Lifshitz point. The configuration of the transition lines (10, 37) near this point is shown in Figures 2a and 2b. The two lines possess a common tangent at the Lifshitz point and form an acute angle if $G_1(K - 1) > 1$, or an obtuse angle for $G_1(K - 1) < 1$.

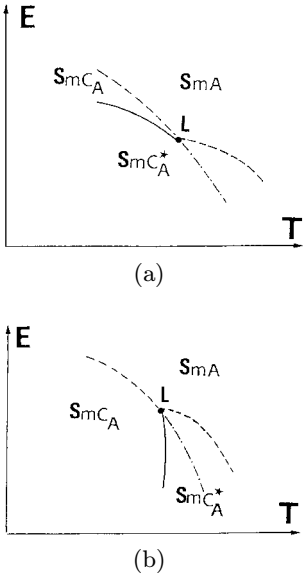

Fig. 2. Electric field-temperature phase diagram in the vicinity of the Lifshitz point, following equations (10, 21, 37); (a) and (b) correspond, respectively, to positive and negative values of $G_1(K - 1) - 1$. Dashed and solid lines have the same meaning as in Figure 1. The dashed-dotted line is the limit of stability line given by equation (10).

Far from the Lifshitz point and from the SmA phase, the approximation (15) does not hold, and the equation of the first order SmC$_{A_1}$–SmC$^*_{A_1}$ transition line has a complex form. However, one can assume that the antiferroelectric order-parameter A_x and A_y go to saturation, and write:

$$A_x = A\cos\psi, \quad A_y = A\sin\psi \tag{38}$$

where A is independent from the space variable u, and $\psi = \psi(u)$.

Let us note that the saturation of A_x and A_y, does not imply a saturation of the ferroelectric components P_x and P_y. This can be foreseen by substituting (38) in the expansion F, defined by equation (5), and by minimizing F with respect to ψ and P_x. One obtains the following equations of states:

$$\frac{\partial^2\psi}{\partial u^2} = -\frac{1}{2}G_2 P_x^2 \sin 2\psi \tag{39}$$

and

$$P_x(1 + G_1 A^2 + G_2 A^2\cos^2\psi) = h. \tag{40}$$

P_x is independent from u, under the condition $G_{1,2}A^2 \ll 1$. Assuming this condition, equation (39), which is analogous to the equations describing the soliton lattice in cholesterics [27], provides the critical field which unwinds the SmC$^*_{A_1}$ helices:

$$h_{cr} = \frac{\pi}{4\sqrt{G_2}}\cdot \tag{41}$$

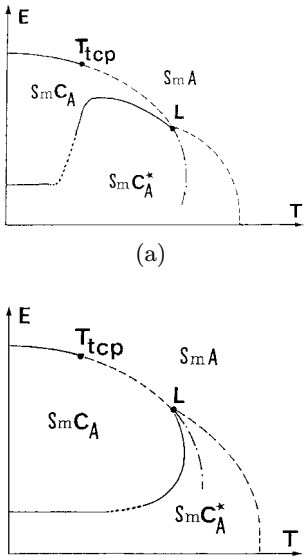

Fig. 3. General configurations of the electric field-temperature phase diagram, for a positive (a) or negative (b) sign of $G_1(K-1)-1$. The direction of the first-order transition line SmC_A–SmC^*_A, far from the SmA phase is deduced from equation (43). The lines have the same meaning as in Figure 2.

Comparing (41) to (13, 28), one can deduce that:

$$h_{cr} < h_L < h_{tcp} \tag{42}$$

i.e. the unwinding critical field is smaller than the field at which the Lifshitz point takes place. In unrenormalized variables, equation (41) becomes:

$$E_{cr} = \pi\lambda_2\alpha_1(4\sqrt{g_2\gamma_2})^{-1}. \tag{43}$$

Assuming that α_1 is independent from temperature, one can deduce from equation (43) that the first-order SmC_{A_1}–$SmC^*_{A_1}$ transition line is parallel to the temperature axis in the saturated regime region of the $T-\mathbf{E}$ phase diagram.

We are now able to give an almost complete description of the topology of the $T-\mathbf{E}$ phase diagram. Thus for fields $-h_L < h < h_L$, one has a second-order SmA–SmC^*_A transition line, given by equation (26). For fields $h_L < h < h_{tcp}$ one has a second-order SmA–SmC_{A_1} transition line, given by equation (10). The two preceding lines merge at the Lifshitz point with the first-order SmC_{A_1}–$SmC^*_{A_1}$ transition line expressed by equation (37). Going back to the unrenormalized variables, given by equation (4), one gets the $T-\mathbf{E}$ phase diagrams, which are shown in Figures 3a and b. Let us note that while the forms of the lines in Figure 3 depend on specific assumptions made in the course of our calculations, the topology of the phase diagrams, namely the sequences of phases, the order of the transitions, the singular points..., are deduced from the symmetry of the system and constitute intrinsic properties of antiferroelectric liquid-crystals. In particular, if one assumes the stabilization of the SmC_{A_2} phase, instead of SmC_{A_1}, similar results are obtained, *i.e.* the potential (16) remains unchanged providing the following transformations.

$$(G_1, G_2) \to (G_1 + G_2, -G_2), \quad \text{and} \quad (\hat{a}_1, \hat{a}_2) \to (\hat{b}_2, \hat{b}_1) \tag{44}$$

$\hat{b}_1$ and $\hat{b}_2$ being perturbative amplitudes defined by:

$$A_x = A_{x2} + \hat{b}_1 \cos qu, \quad \text{and} \quad A_y = \hat{b}_2 \sin qu. \tag{45}$$

4 Induced ferrielectricity in the smectic SmC_A phases

A comparison of the theoretical results found in Section 3, with the temperature-electric field phase diagrams reported experimentally [14–18] requires a more detailed analysis of the *local structure* of the SmC_{A_1}, SmC_{A_2}, and of their incommensurate variants $SmC^*_{A_1}$, and $SmC^*_{A_2}$ phases. With that goal, let us write, in agreement with the definitions given at the beginning of Section 2:

$$\boldsymbol{\eta}_i = \frac{1}{2}(-\sin 2\theta_i \sin\phi_i, \sin 2\theta_i \cos\phi_i)(i = 1, 2) \tag{46}$$

where the η_i are expressed in functions of the tilt angles θ_i and azimuthal angles ϕ_i of two adjacent layers. One can also write:

$$\boldsymbol{\eta}_1 = \frac{1}{2}(\boldsymbol{\eta}_p + \boldsymbol{\eta}_A) \quad \text{and} \quad \boldsymbol{\eta}_2 = \frac{1}{2}(\boldsymbol{\eta}_p - \boldsymbol{\eta}_A) \tag{47}$$

which yields: $\eta_i^2 = \frac{1}{4}\sin^2 2\theta_i$.

Since the polarization $\mathbf{p}$ and antipolarization $\mathbf{a}$ transform respectively as $\boldsymbol{\eta}_p$ and $\boldsymbol{\eta}_A$ under the action of the symmetry group G_0, the bilinear invariants $(\mathbf{p}\cdot\boldsymbol{\eta}_p)$ and $(\mathbf{a}\cdot\boldsymbol{\eta}_A)$ are allowed by the symmetry of G_0. Therefore one can take $\boldsymbol{\eta}_p = K_1\mathbf{p}$ and $\boldsymbol{\eta}_A = K_2\mathbf{a}$, where K_1 and K_2 are constants. Let us first consider the structure of the SmC_{A_1} phase. In this phase, following equation (6), $\boldsymbol{\eta}_p$ is perpendicular to $\boldsymbol{\eta}_A$ so one has: $\boldsymbol{\eta}_A\cdot\boldsymbol{\eta}_p = \eta_1^2 - \eta_2^2 = (1/4)(\sin^2 2\theta_1 - \sin^2 2\theta_2) = 0$. Thus, the tilt angle is the same for two adjacent layers ($\theta_1 = \theta_2 = 0$). Since $\boldsymbol{\eta}_1\cdot\boldsymbol{\eta}_2 = (1/4)\sin^2 2\theta\cos(\phi_1 - \phi_2)$, one finds the following difference for the azimuthal angles of two successive layers:

$$\phi_1 - \phi_2 = \ \arccos\ (\eta_p^2 - \eta_A^2)/(\eta_p^2 + \eta_A^2). \tag{48}$$

In the SmA phase, under applied field, one has: $\eta_A = 0$, $\phi_1 = \phi_2$. In the vicinity of the SmA–SmC_{A_1} transition line, η_A will remain small, and equation (48) can be approximated by: $\phi_1 - \phi_2 \simeq 2|\boldsymbol{\eta}_A|/|\boldsymbol{\eta}_p|$. The corresponding structure of the SmC_{A_1} phase is represented in Figure 4a. It shows the application of an electric field *modifies the antiferroelectric structure of the SmC_{A_1} phase, inducing a ferrielectric ordering of the molecular dipoles.*

A different situation occurs for the structure of the SmC_{A_2} phase when an electric field is applied, as it is

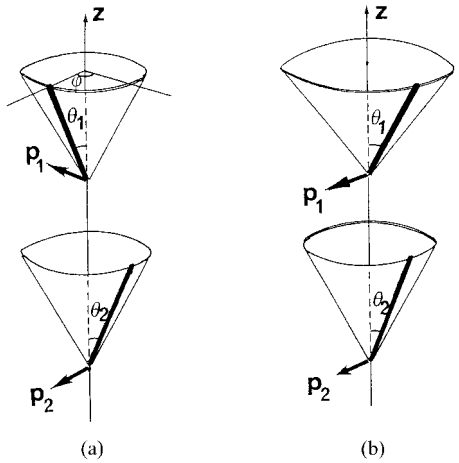

Fig. 4. Representation of the structures of two adjacent layers in the SmC_{A_1} (a) and SmC_{A_2} (b) phases. The description of the structures is given in the text. In (a) one has $\theta_1 = \theta_2$ and $|\mathbf{P}_1| = |\mathbf{P}_2|$, whereas in (b) $\theta_1 \neq \theta_2 |\mathbf{P}_1| \parallel |\mathbf{P}_2|, |\mathbf{P}_1| \neq |\mathbf{P}_2|$.

illustrated in Figure 4b. In this phase one has, following (7): $\boldsymbol{\eta}_p \parallel \boldsymbol{\eta}_A$, and thus: $\boldsymbol{\eta}_p \wedge \boldsymbol{\eta}_A = 2\boldsymbol{\eta}_1 \wedge \boldsymbol{\eta}_2 \sim 2\sin(\phi_1 - \phi_2) = 0$, so that the azimuthal angles of two adjacent layers are equal ($\phi_1 = \phi_2 = \phi$) whereas the tilt angles verify:

$$\sin 2\theta_1 = 2(|\boldsymbol{\eta}_p| + |\boldsymbol{\eta}_A|), \quad \text{and} \quad \sin 2\theta_2 = 2(|\boldsymbol{\eta}_p| - |\boldsymbol{\eta}_A|). \tag{49}$$

From the condition that $\boldsymbol{\eta}_A = 0$ in the SmA phase, one gets here: $\theta_1 = \theta_2 = 0$ and $\sin 2\theta = 2|\boldsymbol{\eta}_p|$. Close to the SmA–$SmC_{A_2}$ transition, in the SmC_{A_2} phase one can assume $\theta_1 + \theta_2 \sim 2\theta$ and consequently:

$$\theta_1 - \theta_2 \sim 2\theta |\boldsymbol{\eta}_A| (1 - 4\eta_p^2)^{-1/2}. \tag{50}$$

The structure of the SmC_{A_2} phase is shown in Figure 4b. It is characterized, under applied electric field, by a *ferrielectric* ordering of the dipoles *which differs from the ferrielectric order found in the SmC_{A_1} phase*, the two structures being differentiated only when the field is applied.

Let us now analyze the local structure of the SmC_A^* phase. At zero field one has $\boldsymbol{\eta}_p = 0$, $\boldsymbol{\eta}_1 = -\boldsymbol{\eta}_2$ and $\boldsymbol{\eta}_A = 2\boldsymbol{\eta}_1$. Thus $|\boldsymbol{\eta}_A| = \sin 2\theta_1 = \sin 2\theta_2 = \pm K_2 \left[-(\alpha_2 - \lambda_2^2/4g_2)/\beta_2\right]^{1/2}$ and $\phi_1 = \phi_2 + \pi$. The corresponding helicoidal structure is represented in Figure 5a. Under applied field, using the equilibrium values of the order-parameter components given by equation (15), in which we take $\omega = \pi/2$, one can assume near the Lifshitz point that the polarization amplitudes $\hat{p}_1$ and $\hat{p}_2$ can be neglected in equation (15), and that $A_{y_1} = 0$. Accordingly:

$$\eta_{p_x} \simeq \eta_0,\ \eta_{p_y} \simeq 0,\ \eta_{A_x} \simeq \tilde{\eta}_1 \cos qu,\ \eta_{A_y} \simeq \tilde{\eta}_2 \sin qu \tag{51}$$

which yield, using (4):

$$\eta_0 = P_x \lambda_2^2 g_2^{-1} (\beta_2 \alpha_1)^{1/2} K_1, \text{ and } \tilde{\eta}_{1,2} = \hat{a}_{1,2} \lambda_2 (\beta_2 g_2)^{-1/2} K_2$$

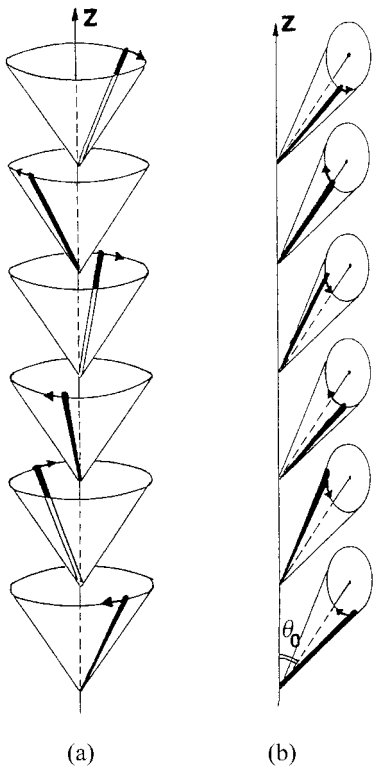

Fig. 5. Representation of the structures of two adjacent layers in the SmC_A^* phase at zero electric field (a) and under large fields (b). The description of the structures is given in the text.

where $P_x = h$ and $\hat{a}_{1,2}$ are given by equation (35). From (49) one obtains the angles θ_i and $\phi_i (i = 1, 2)$ in the SmC_A^* phase:

$$\phi_{1,2} = \frac{\pi}{2} - \arcsin\left[\pm \sin qu [(\eta_0 \pm \tilde{\eta}_1 \cos qu)^2 + \tilde{\eta}_2 \sin^2 qu]^{1/2}\right] \tag{52}$$

$$\phi_{1,2} = \arcsin\left[\pm [\eta_0^2 + \tilde{\eta}_1^2 \cos^2 qu + \tilde{\eta}_2^2 \sin^2 qu \pm 2\eta_0 \tilde{\eta}_1 \cos qu]^{1/2}\right] \tag{53}$$

where the signs (+) and (−) in (52, 53) correspond respectively to (ϕ_1, θ_1) and (ϕ_2, θ_2). Under small fields $G_2 h^2 \ll 1$ one has $\tilde{\eta}_1 \simeq \tilde{\eta}_2 = \tilde{\eta} \gg \eta_0$, which yields the following approximative values:

$$\phi_{1,2} \simeq \pm\frac{\pi}{2} - qu + \eta_0 \tilde{\eta}^{-1} \sin qu, \text{ and } \theta_{1,2} \simeq \frac{1}{2} \arcsin(\tilde{\eta}) \tag{54}$$

corresponding to a *slightly distorted helix* in which the azimuthal rotation of the molecules takes place non uniformly with respect to *z: the rotation is periodically accelerated in one layer and decelerated in the adjacent layer.* In this case the tilt angle is essentially determined by the parameter $\tilde{\eta}$.

Under large fields, one has $\eta_0 \gg \tilde{\eta}_i$ and the tilt is determined by η_0. Assuming $\sin 2\theta_0 = \eta_0$ and $\phi_0 = \pi/2$, one can write: $\theta_i = \theta_0 + \delta\theta_i$, and $\phi_i = \phi_0 + \delta\phi_i$, with:

$$\delta\theta_{1,2} = \pm\tilde{\eta}_1 \cos qu(2\cos 2\theta_0)^{-1}, \text{ and } \delta\phi_{1,2} = \pm\tilde{\eta}_2\eta_0^{-1} \sin qu \tag{55}$$

which describes the rotation of the molecules around the average direction $\theta_i = \theta_0$, $\phi_i = \pi/2$. The molecules in two adjacent layers rotate in opposed directions, and turn around an elliptic trajectory as shown in Figure 5b. The ratio of the axes of the ellipse is:

$$r = (1 - G_2h^2)(1 + G_2h^2)^{-1} \cos\theta_0(\cos 2\theta_0)^{-1}.$$

Following the preceding considerations, the structure of the SmC_{A_1}, SmC_{A_2}, and SmC^*_A phases are locally distorted by the application of an electric field, and may appear at the macroscopic level as ferrielectric, or complex antiferroelectric phases. This allows a partial interpretation of some regions of the temperature-electric field phase diagrams, which have been disclosed experimentally in antiferroelectric liquid crystal systems. If the ferroelectric degree of freedom is negligible with respect to the antiferroelectric one, the strong dipolar interaction of the system with the external field, will lead, near to the SmA–SmC^*_A spontaneous transition, to a *simultaneous* unwinding process and field-induced antiferro-ferroelectric transition. Far from the SmA phase, in the low temperature region, the action of the field will first lead to the helix unwinding and then, with increasing field, to a antiferro-ferroelectric transition between unwound structures. However, the preceding scheme will be generally complicated by the existence of additional phases in the phase diagram, giving rise to more complex phase sequences, which are beyond the scope of the present study.

For example, in MHPOBC [14,15] the $T-\mathbf{E}$ phase diagram shows that, with increasing field, the SmC^*_A phase transforms into the SmC^*_γ ferrielectric phase across a line of first-order transitions. The domain of stability of the SmC^*_γ phase is enlarged for larger fields, as for the SmC_{A_1} or SmC_{A_2} phase in Figure 3. However, the comparison cannot go further as the SmC^*_A and the SmC^*_γ phases are separated from the SmA phase, by two additional antiferroelectric (SmC^*_α) and ferroelectric (SmC^*_β) phases. An analogous situation is reported in tolan [18] $\{C_{10}H_{21}O\text{-}O\text{-}C\text{-}C\text{-}O\text{-}COO\text{-}O\text{-}COO\text{-}C^*H(CH_3)\text{-}C_6H_{13}\}$ in which the SmC^*_A phase transforms into the ferrielectric SmC^*_γ phase, with increasing field, the two preceding phases being separated from the SmA phase by a ferroelectric SmC^*_β phase. In TFMHPOBC, no field-induced phase is reported between the SmC^*_A and SmA phases. At last, let us mention the case of 3MC2PCPOPB [17] {4-3(methoxycarbonyl-2-propoxycarbonyl)phenyl 4-(4-(*n*-octyloxy)phenyl)benzoate} in which an unidentified smectic phase, denoted Sm*, is induced at large fields from the SmC^*_A phase. The line of transitions separating the SmC^*_A and Sm* phases merge at a singular point with the SmC*–SmC^*_A transition line, which is found in this substance below the SmA phase. An extension of our work, that would include the SmC* phase as well as ferrielectric phases, is necessary to allow a more detailed interpretation of the $T-\mathbf{E}$ phase diagrams for the preceding compounds.

One of the authors (A.A.B) is grateful to the Alexander von Humboldt foundation for financial support.

References

1. A.D.L. Chandani, E. Gorecka, Y. Ouchi, H. Takezoe, A. Fukuda, Jpn J. Appl. Phys. **28**, L1265 (1989).
2. M. Fukui, H. Orihara, Y. Yamada, N. Yamamoto, Y. Ishibashi, Jpn J. Appl. Phys. **28**, L849 (1989).
3. H. Takezoe, J. Lee, A.D.E. Chandani, E. Gorecka, Y. Ouchi, A. Fukuda, K. Terashima, K. Furukawa, Ferroelectrics **114**, 187 (1991).
4. E. Gorecka, A.D.L. Chandani, Y. Ouchi, H. Takezoe, A. Fukuda, Jpn J. Appl. Phys. **29**, 131 (1990).
5. J. Lee, A.D.L. Chandani, K. Itoh, Y. Ouchi, H. Takezoe, A. Fukuda, Jpn J. Appl. Phys. **29**, 1122 (1990).
6. J. Lee, Y. Ouchi, H. Takezoe, A. Fukuda, J. Watanabe, J. Phys.-Cond. **2**, SA271 (1990).
7. I. Musevic, R. Blinc, B. Zeks, M. Copic, M.M. Wittebrood, Th. Rasing, H. Orihara, Y. Ishibashi, Phys. Rev. Lett. **71**, 1180 (1993).
8. K. Tajiri *et al.* (unpublished).
9. H. Sun, H. Orihara, Y. Ishibashi, J. Phys. Soc. Jpn **60**, 4175 (1991).
10. S. Hiller, S.A. Pikin, W. Haase, J.W. Goodby, I. Nishiyama, Jpn J. Appl. Phys. **33**, L1170 (1994).
11. S. Hiller, S.A. Pikin, W. Haase, J.W. Goodby, I. Nishiyama, Jpn J. **33**, L1096 (1994).
12. M. Glogarova, H. Sverenyak, H.T. Nguyen, C. Destrade, Ferroelectrics (to appear).
13. K. Hiraoka, H. Takezoe, A. Fukuda, Ferroelectrics (to be published).
14. T. Isozaki, T. Fujikawa, H. Takezoe, A. Fukuda, T. Hagiwara, Y. Suzuki, I. Kawamura, Jpn J. Appl. Phys. **31**, L1435 (1992).
15. J. Hatano, M. Harazaki, M. Sato, K. Iwauchi, S. Saito, K. Murashiro, Jpn J. Appl. Phys. **32**, 4344 (1993).
16. T. Fujikawa, H. Orihara, Y. Ishibashi, Y. Yamada, Y. Yamamoto, K. Mori, K. Nakamura, Y. Suzuki, T. Hagiwara, I. Kawamura, Jpn J. Appl. Phys. **30**, 2826 (1991).
17. H. Moritake, N. Shigeno, M. Ozaki, K. Yoshino, Jpn J. Appl. Phys. **31**, 3193 (1992).
18. J. Pavel, P. Gisse, H.T. Nguyen, Ph. Martinot-Lagarde, Ferroelectrics (to be published).
19. J. Li, H. Takezoe, A. Fukuda, Jpn J. Appl. Phys. **30**, 532 (1991).
20. H. Orihara, Y. Ishibashi, Jpn J. Appl. Phys. **29**, L115 (1990).
21. V.L. Lorman, A.A. Bulbitch, P. Tolédano, Phys. Rev. E **49**, 1367 (1994).
22. B. Zeks, R. Blinc, M. Cepic, Ferroelectrics **122**, 221 (1991).
23. H. Orihara, Y. Ishibashi (unpublished).
24. J.C. Tolédano, P. Tolédano, *The Landau Theory of Phase Transitions*, Chap. 5 (World Scientific, Singapore, 1987).
25. R.M. Hornreich, M. Luban, S. Shtrikman, Phys. Rev. Lett. **35**, 1678 (1975).
26. A. Michelson, D. Cabib, J. Phys. Lett. (Paris) **38**, L321 (1977).
27. P.G. de Gennes, J. Prost, *The Physics of Liquid Crystals*, Chap. 6 (Clarendon, Oxford, 1993).